PERGAMON

Deep-Sea Research II 46 (1999) 885–906

DEEP-SEA RESEARCH
PART II

Rates of particle scavenging and particulate organic carbon export estimated using ^{234}Th as a tracer in the subtropical and equatorial Atlantic Ocean

Matthew A. Charette*,[1], S. Bradley Moran

Graduate School of Oceanography, University of Rhode Island, Narragansett, RI 02882-1197, USA

Received 3 September 1997; received in revised form 24 February 1998; accepted 15 March 1998

Abstract

The export flux of particulate organic carbon and particle scavenging rates were calculated using a ^{234}Th-based approach along a transect through the mid-Atlantic from 35°S to 10°N during May and June of 1996. The median residence time of dissolved ^{234}Th along the transect was 135 days, with intense scavenging from 5°N to 6°N ($\bar{\tau}_d = 86 \pm 17$ days). Vertical profiles and depth-integrated samples (surface-100 m) of dissolved (< 0.7-μm), suspended particulate (0.7–53-μm), and large particulate (> 53-μm) ^{234}Th activities were collected to estimate export fluxes of particulate organic carbon (POC). A steady-state model of the ^{234}Th activity balance in the upper 100 m was combined with measurements of the POC/^{234}Th ratio on > 53-μm particles. POC export ranged from 3.2 mmol C m^{-2} d^{-1} in the central South Atlantic to 43 mmol C m^{-2} d^{-1} at 2.5°S. Export production along the Atlantic equator (5°S–5°N, 25°E–5°W) is estimated to be 0.29 Gt C yr^{-1}. The ^{234}Th-derived POC export estimates reported here and from other studies are comparable with model simulations of export production from the Princeton General Circulation Model (GCM) for the Atlantic Ocean.

1. Introduction

Our understanding of particulate organic carbon (POC) fluxes in subtropical and equatorial upwelling regions of the global ocean has been gained from process studies

* Corresponding author. Tel.: + (508) 289-3205; fax: + (508) 457-2193.
[1] Present address: Woods Hole Oceanographic Institution, Woods Hole, MA 02543, USA.
E-mail address: mcharrette@whoi.edu (M.A. Charette)

0967-0645/99/$ - see front matter
PII: S0967-0645(99)00006-5

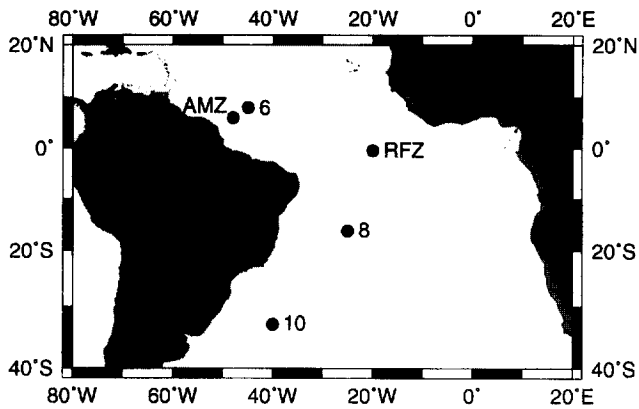

Fig. 1. Map of the IOC-96 cruise track and station locations.

such as the US JGOFS EqPac program (Murray et al., 1994) and from simulations using General Circulation Models (GCMs) (Najjar et al., 1992). In the tropical Atlantic, much of our knowledge of biological processes has come from programs such as the First Global Atmospheric Research Program Global Experiment (FGGE) in 1979, Seasonal Equatorial Atlantic Experiment (SEQUAL-FOCAL) in 1983–1984, from applications of the coastal zone color scanner (CZCS), and from individual field programs (Bishop et al., 1977). These studies have improved our knowledge of variations in nutrient distributions and of the influence of different physical processes on such distributions in the Atlantic. However, other than model simulations, there are few direct estimates of POC export in the subtropical and equatorial Atlantic.

^{234}Th ($t_{1/2}$ = 24.1 d) is a naturally occurring, particle-reactive radionuclide that is produced in situ from its soluble parent ^{238}U ($t_{1/2} = 4.47 \times 10^9$ yr). Early investigations reported the existence of ^{234}Th/^{238}U disequilibrium in the upper ocean and attributed this to scavenging and particle export (Bhat et al., 1969; Matsumoto, 1975). Subsequent studies (Coale and Bruland, 1985,1987; Bruland and Coale, 1986) demonstrated that ^{234}Th scavenging was controlled by the rate of biogenic particle production and export. More recent studies have utilized ^{234}Th as a tracer of the export flux of POC in a wide range of oceanic regimes (Buesseler et al., 1992a,1995; Cochran et al., 1995; Murray et al., 1996; Bacon et al., 1996; Rutgers van der Loeff et al., 1997; Moran et al., 1997). In this paper, we report measurements of ^{234}Th/^{238}U disequilibrium along a transect from 35°S to 10°N in the Atlantic Ocean (Fig. 1) and use these data to calculate rates of particle scavenging and POC export.

2. Methods

2.1. Sampling

Samples were collected aboard the R/V *Knorr* from May 18 to June 20, 1996. Large-volume samples were collected in three ways: (1) with a rosette configured for

200-l samples; (2) from a deck pump for samples less than 20 m deep, and; (3) from the ship's PVC seawater intake system for surface samples (~ 3 m) during transit. In the first two cases, 200–600 l of seawater were passed at 3–5 $l\,min^{-1}$ sequentially through a 142-mm dia. PVC filter holder with a 53-μm Nitex screen and a 0.7-μm Poretics GF-75 glass fiber filter (Pike and Moran, 1997), and two MnO_2 impregnated cartridges connected in series to scavenge dissolved ^{234}Th (Hartman and Buesseler, 1994). The collection efficiency of the MnO_2 cartridges was calculated using,

$$E = 1 - \frac{\mathrm{MnB}}{\mathrm{MnA}} \tag{1}$$

where MnA and MnB are the decay-corrected activities of ^{234}Th on the first and second cartridges, respectively (Livingston and Cochran, 1987). In the third case, when sampling from the ship's intake, 800–2000 l at flow rates of 4–14 $l\,min^{-1}$ were passed through a 1-μm pore size Hytrex II prefilter to collect the particulate ^{234}Th, and dissolved ^{234}Th was collected on the MnO_2-impregnated cartridges.

Large-volume samples were collected at depth by deploying a rosette configured with six 30-l and two 10-l Niskin bottles (200 l). Tygon tubing was then connected to the Niskin's spigots to form an "octopus" and the seawater was pumped at ~ 5 $l\,min^{-1}$ through the 142-mm filter holder and two MnO_2 cartridges. The rosette sampling was conducted 2–3 times per depth. Samples (200 to 500 l) from the upper 20 m were collected using a deck pump. For each profile station, sample collection was completed within 12–15 h. To obtain better sampling resolution about the equator, depth-integrated water samples were collected at several locations from 10°S to 8°N. In this case, the rosette was deployed 1–2 times to a depth of 500 m and bottles tripped at 20 m intervals between 100 m and the surface.

2.2. ^{234}Th analyses

^{234}Th activities were measured in the MnO_2 cartridges and the GF-75 filters at sea by gamma spectrometry (63.3 keV peak; 0.03 cpm background) using a Canberra pure-Ge planar detector (2000 mm^2 active area; Buesseler et al., 1992b). Samples from the ship's intake and on the Nitex screens were counted in the shore-based lab. The prefilter and MnO_2 cartridges from the ship's intake were ashed at 500°C for ~ 6 h and ^{234}Th measured with a Canberra pure-Ge well detector (V = 150 cm^3; 0.09 cpm background). Nitex particulate ^{234}Th (> 53 μm) was quantified by low-background beta counting (background = 0.12–0.34 cpm) with a RISØ gas-flow Geiger-Müller counter operating in anti-coincidence mode. Two 25-mm subsamples from the GF-75 filters were stored frozen for POC analysis. The remainder of the filter was folded and dried in a 47 mm polystyrene petri dish at 60°C. Filters in this geometry were counted to ⩽ 10% error using the planar detector, which typically required ~ 4 h. The detector efficiency for a folded GF-75 was 17 ± 6%, determined from filters spiked with NIST ^{238}U (SRM #4321B).

The Nitex screens were sonicated for two minutes in 100 ml of filtered seawater to resuspend the large particles. The Nitex screen was removed and rinsed to dislodge any remaining particles. The resulting solution was filtered through a precombusted

25-mm Whatman QM-A (pore size 1.2 μm) and stored frozen. Once in the lab, the filters were dried overnight at 60°C. After cutting a wedge (10–20% by weight) for POC analyses, the filter was mounted on an acrylic planchet and covered with Al foil (9 mg m^{-2}), which shielded alpha particles and low energy beta-emitters. ^{234}Th was quantified by counting the daughter ^{234m}Pa ($t_{1/2}$ = 1.2 min). Each beta detector was individually calibrated and detector efficiencies under these conditions ranged in 23–27%. Samples were counted once each week for four cycles (1 cycle = 1000 min). These data were fitted to the 24.1-day half-life of ^{234}Th and decay corrected to the mid-point of sampling.

A 5-ton press was used to crush the MnO_2 cartridges into a reproducible geometry (height = 3 cm). After crushing, the MnA cartridges were counted for 3–7 h to $\leqslant 5\%$ error and the MnB cartridges were counted for 4–14 h to $\sim 15\%$. The detector efficiency at 63.3 keV for a crushed cartridge was 6.3%, which was determined by counting a cartridge with the same geometry that was spiked with a known quantity of ^{234}Th. All samples were decay-corrected to the midpoint of sampling, and backgrounds were subtracted. The activity of dissolved ^{234}Th ($^{234}Th_d$) was calculated from the formula:

$$^{234}Th_d = \frac{^{234}Th_A}{E \times V} \tag{2}$$

where $^{234}Th_A$ is the activity on the MnA cartridge, E is the collection efficiency, and V is the volume processed. ^{238}U was estimated from salinity using the relationship from Chen et al. (1986), $^{238}U = 0.07081 \times S(‰)$. In deep waters ($> 150$ m) where ^{234}Th should be secular equilibrium with ^{238}U, $^{234}Th/^{238}U$ activity ratios averaged 0.996 ± 0.054 ($n = 11$), which is consistent with our independent calibration using the ^{238}U standard.

2.3. Particulate organic carbon and nitrogen

POC and particulate organic nitrogen (PON) were determined using a Carlo Erba EA-1108 CHN Analyzer. Frozen samples were dried at 60°C for 12 h. A pie-shaped wedge (10–20% of the filter by weight) was cut from each filter. To remove inorganic carbon ($CaCO_3$), subsamples were placed in a desiccator and fumed with concentrated HCl. The subsamples were again dried, placed in precleaned tin boats, and pelletized. Field and lab filter blanks (QMA and GF-75) were analyzed every 10 samples. Field blanks were quantified by randomly stacking two filters and measuring the carbon and nitrogen on the second filter, which accounted for approximately 10% of the measured POC and PON concentration.

3. Results

3.1. Collection efficiency of the MnO_2 cartridges

The relationship between the collection efficiency of the MnO_2 cartridges and flow rate and volume processed was examined using samples from the ship's intake system.

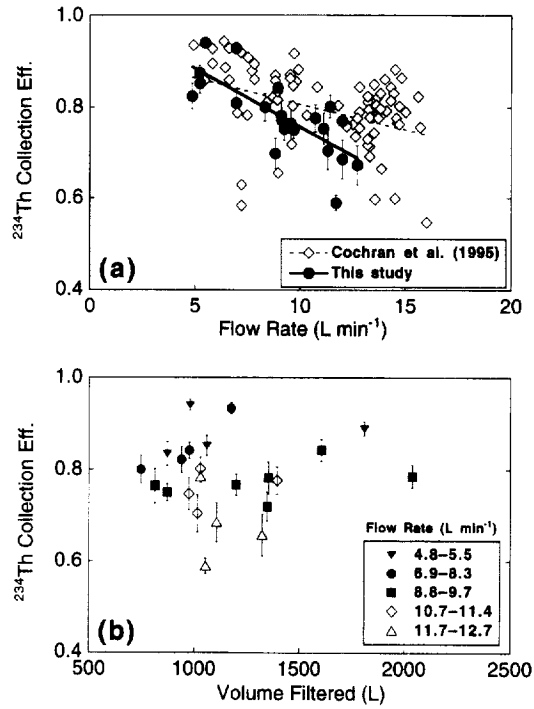

Fig. 2. (a) Dependence of MnO_2 cartridge collection efficiency on flow rate. (b) Relationship between MnO_2 cartridge collection efficiency and total volume processed.

We were concerned with two issues: (1) increased flow rates may reduce the scavenging efficiency, and; (2) the collection efficiency may decline as adsorption sites for ^{234}Th on the MnA cartridge become saturated. To test these hypotheses, the flow rate was varied from approximately 4.8–13 l min^{-1} using a ball valve, and $\sim$ 750–2000 l of seawater was processed. The resulting collection efficiencies for ^{234}Th ranged from 59 to 94%, with a mean of 79 $\pm$ 8.3%. We observed an inverse relationship between flow rate and efficiency (Fig. 2a). Also observed by Cochran et al. (1995), the decrease in collection efficiency with flow rate suggests that adsorption of ^{234}Th on the MnO_2 cartridge is limited kinetically. The difference between the two slopes may be attributed to differences in the loading of MnO_2 onto the cartridge, which is a function of the method used to prepare them.

One characteristic of the MnO_2 cartridge not previously documented is that collection efficiency does not depend on volume; we were interested in learning whether E decreased with an increase in the volume of seawater filtered (Fig. 2b). There was no such observed trend given our limited data set ($n = 23$). Data were grouped to ensure that the absence of a trend was not an artifact of flow rate, in fact, two of the three samples that exceeded 1500 l had intermediate flow rates. These results suggest that ^{234}Th adsorption sites for a 8.5 cm cartridge are not saturated at

volumes equaling or below 2000 l, which is essentially equivalent to pumping 6000 l through the more commonly used 25 cm cartridges. This result implies that when large volumes ($\sim$ 1000 l) of seawater are available, the analytical signal for the short-lived ^{234}Th can be increased without a significant loss in collection efficiency for 8.5 cm MnO_2 cartridges.

3.2. ^{234}Th in the surface waters

Total ^{234}Th (particulate + dissolved) results in the surface waters indicate relatively little particle scavenging and export along the cruise track (Table 1). ^{234}Th:^{238}U activity ratios (AR) ranged from 0.98 at 25°S to 0.67 at 5°N. From 10°S to 8°N, the average deficit of ^{234}Th relative to ^{238}U was 0.50 dpm l^{-1}; only at 6°S did the total ^{234}Th activity approach secular equilibrium with ^{238}U. The greatest removal of ^{234}Th occurred between 5°N and 6°N ($n = 3$), where the average total ^{234}Th activity was 1.78 ± 0.11 dpm l^{-1} (AR = 0.72).

3.3. ^{234}Th profiles

In Fig. 3, we present depth profiles of ^{234}Th along with nutrients, pigments, and dissolved oxygen, temperature and POC. At each station, there existed a net depletion of ^{234}Th relative to the parent ^{238}U (Table 2). There were several interesting differences between the stations.

At Station 10, located in the Brazil Current at 33°S, we found export of ^{234}Th to be low. At 50 m, there existed a small deficit of 0.40 dpm l^{-1} relative to the parent ^{238}U. At Station 8, the euphotic zone extended well below the mixed layer (80 m), as evidenced by the broad pigment maximum centered at 140 m. At Stations 10 and 8, the maximum ^{234}Th export was confined to deeper layers.

At Station RFZ, scavenging and particle export removal was evident within the upper 20 m. The particulate ^{234}Th maximum at 20 m coincided with the minimum in dissolved ^{234}Th, indicating intense scavenging. In contrast, a ^{234}Th remineralization peak was observed at 100 m, equivalent to an activity ratio of 1.14. Where regeneration and rapid export of particles balance each other (50 m), ^{234}Th was in equilibrium with ^{238}U.

At Station 6, we observed ^{234}Th/^{238}U disequilibria throughout the water column to 150 m. Export of ^{234}Th was highest at the surface and decreased with depth. At Station AMZ, located over 200 km from the coastline, we encountered a surface plume containing a thin lens of Amazon River water. The lens was a 0.5–1 m thick layer of turbid water that had a salinity nearly 10 ppt less than the water below. Here, silicate concentrations were 25 to 30 times above ambient concentrations – a clear indication of Amazon River water. The lowest total ^{234}Th signal was found at this station at this depth. Aside from the low ^{234}Th in the Amazon plume, the profile most resembles that from IOC Station 6.

Particulate ^{234}Th in the two size classes was characterized by a subsurface maximum followed by a monotonic decrease with depth (Fig. 4a and b). Depth profiles of the $>$ 53-μm size-fraction showed more scatter than ^{234}Th in the 0.7–53-μm size class.

Table 1

^{234}Th activities, particulate and dissolved residence times, and the dissolved ^{234}Th scavenging rate coefficient in surface waters (~ 3 m) of the subtropical and tropical Atlantic ocean

Lat (deg N)	Long (deg W)	Diss. ^{234}Th (dpm l^{-1})	± error	Part. ^{234}Th (dpm l^{-1})	± error	Total ^{234}Th (dpm l^{-1})	± error	^{238}U (dpm l^{-1})	τ_d (days)	τ_p (days)	k† (days^{-1})
8	45.0	2.02	0.09	0.056	0.006	2.07	0.09	2.51	141	4.4	0.0071
7.3	40.1	2.07	0.10	0.066	0.005	2.13	0.10	2.52	158	5.9	0.0063
6.6	36.2	2.08	0.12	0.047	0.006	2.13	0.12	2.51	169	4.3	0.0059
6	32.0	1.81	0.08	0.020	0.003	1.83	0.08	2.48	94	1.1	0.0106
5.3	27.8	1.81	0.10	0.042	0.005	1.86	0.10	2.47	96	2.4	0.0104
5.2	26.8	1.62	0.08	0.040	0.005	1.66	0.08	2.46	66	1.7	0.0150
4.6	22.8	1.95	0.12	0.085	0.006	2.04	0.12	2.46	135	7.1	0.0074
3.6	22.0	1.98	0.12	0.069	0.004	2.04	0.13	2.44	148	6.1	0.0068
2.7	21.6	2.14	0.14	0.047	0.006	2.18	0.14	2.44	248	6.5	0.0040
− 0.2	20.0	1.89	0.11	0.082	0.006	1.97	0.11	2.44	119	6.1	0.0084
− 1.4	20.0	1.86	0.11	0.057	0.006	1.92	0.11	2.51	101	3.4	0.0099
− 2.7	20.8	1.81	0.13	0.048	0.005	1.86	0.13	2.50	91	2.6	0.0110
− 5.3	21.3	1.88	0.10	0.039	0.006	1.92	0.10	2.50	106	2.3	0.0094
− 6.2	21.8	2.34	0.18	0.052	0.007	2.40	0.18	2.52	460	14.5	0.0022
− 9.8	22.8	1.87	0.10	0.093	0.006	1.97	0.10	2.55	96	5.5	0.0104
− 11.1	23.2	1.91	0.08	0.073	0.003	1.99	0.08	2.55	105	4.5	0.0095
− 13.5	23.9	1.88	0.16	0.134	0.009	2.01	0.16	2.59	92	8.1	0.0109
− 23.7	31.5	1.94	0.10	0.158	0.007	2.10	0.10	2.58	105	11.4	0.0095
− 25.4	33.3	2.33	0.14	0.180	0.026	2.51	0.14	2.56	352	126.1	0.0028
− 28.9	37.0	2.14	0.14	0.062	0.008	2.21	0.14	2.53	193	6.6	0.0052
− 30.2	37.6	2.05	0.08	0.136	0.020	2.19	0.09	2.52	152	14.2	0.0066
− 33.1	40.4	2.26	0.14	0.136	0.012	2.39	0.14	2.52	300	37.7	0.0033
− 33.8	46.3	2.22	0.18	0.179	0.021	2.40	0.19	2.52	254	50.1	0.0039

Errors for ^{234}Th were propagated from counting statistics and Mn cartridge collection efficiency (for dissolved ^{234}Th).

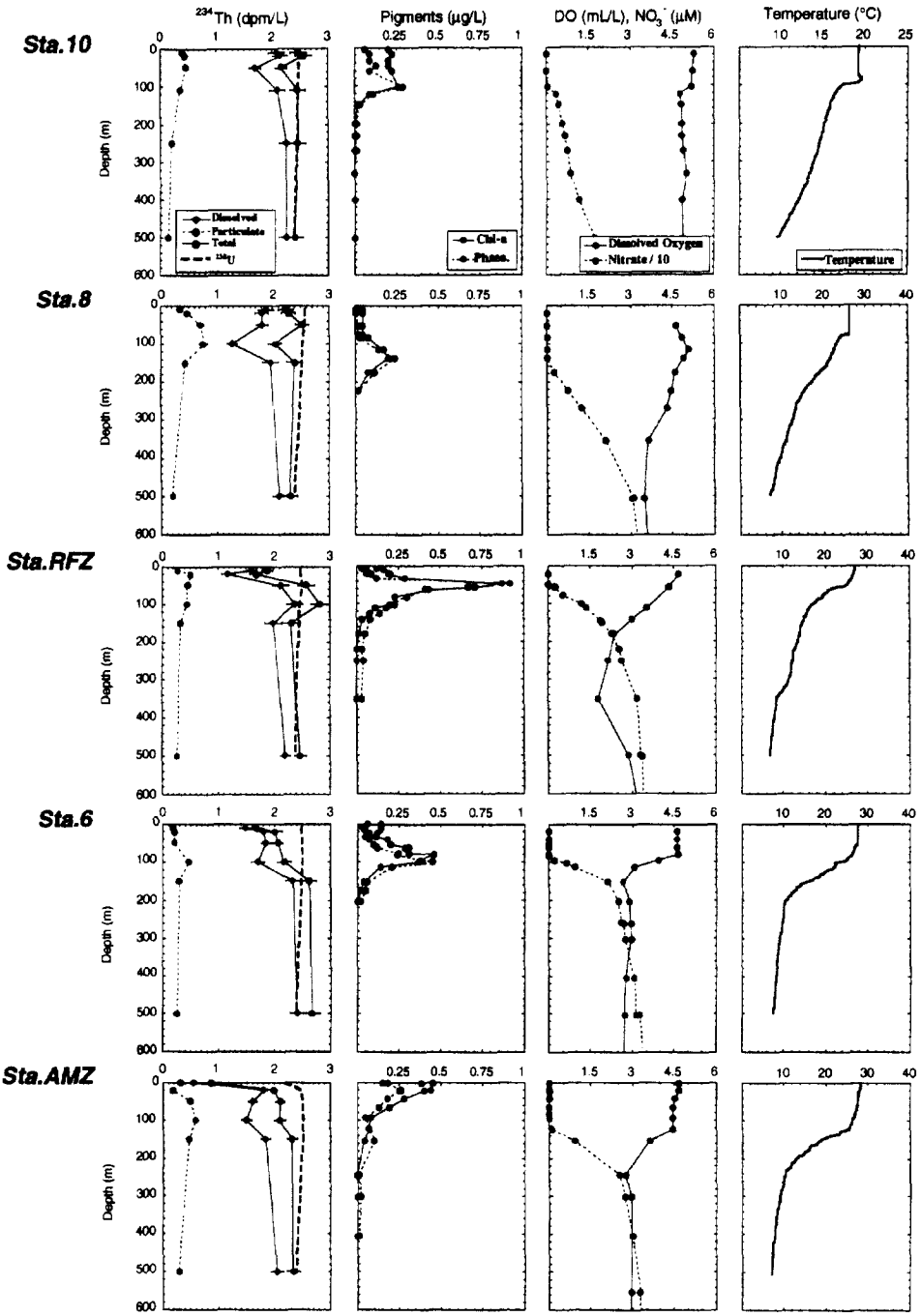

Fig. 3. Vertical profiles of ^{234}Th, pigments, nitrate, dissolved oxygen, and temperature. Error bars for ^{234}Th were propagated from counting statistics and calibration uncertainty.

The > 53-μm fraction ranged from 1 to 10% and averaged 3% of the total particulate ^{234}Th. The ^{234}Th activity of the large particles ranged from 0.0015 to 0.014 dpm l^{-1}, which compares with 0.13 to 0.76 dpm l^{-1} in the 0.7–53-μm size fraction.

Data from the depth-integrated water samples (0–100 m) at seven stations from 10°S to 8°N are presented in Table 3. At two stations, 10°S and 2.5°N, ^{234}Th was in equilibrium with ^{238}U, whereas the ^{234}Th/^{238}U activity ratio ranged from 0.73 to 0.92 for all other samples. Approximately 10–22% of the total ^{234}Th was in particulate form.

3.4. Distribution of particulate organic carbon

The distribution of suspended (0.7–53-μm) and sinking (> 53 μm) POC was characterized by maximum values in the near-surface waters (Fig. 4c and d). POC concentrations ranged from 1.5 to 5.0 μM in the surface waters and decreased with depth to values of 0.47–0.74 μM at 500 m. Profiles of the > 53-μm POC with depth exhibited a similar distribution, with low concentrations and subsurface maxima (20 m) at stations south of the equator. Shallow maximas (1–10 m) were apparent at stations north of the equator. We found a wide range of > 53 μm concentrations in the surface waters, from 0.047 μM at Station 8 (10 m) to 1.5 μM at Station RFZ (20 m); at 500 m this range narrowed from 0.028 (St. 6) to 0.095 μM (Station 10). The shallow maximum in > 53 μm POC at St. RFZ comprised 24% of the total POC (suspended + sinking), which coincided with a minimum in dissolved ^{234}Th at this station.

4. Discussion

4.1. Residence time of ^{234}Th in the surface waters

The mean lifetime of ^{234}Th (34.8 d) makes it a useful tool for calculating residence times of particles, as well as particle fluxes, on a time-scale of days to weeks. Assuming steady-state removal and neglecting horizontal advection, the activity balance of dissolved ^{234}Th is given by,

$$J_{Th} = A_U\lambda_{Th} - A^d_{Th}\lambda_{Th} \quad (3)$$

where A_U is the ^{238}U activity (^{238}U = 0.07081 × S[‰]; Chen et al., 1986), λ_{Th} is the ^{234}Th decay constant (0.0288 d^{-1}), and A^d_{Th} is the dissolved ^{234}Th activity. The first term ($A_U\lambda_{Th}$) represents the production of ^{234}Th from ^{238}U. The second term ($A^d_{Th}\lambda_{Th}$) is the loss of dissolved ^{234}Th by radioactive decay. The term J_{Th} is the net flux of dissolved ^{234}Th. In a similar manner, the particulate flux of ^{234}Th can be expressed as,

$$P_{Th} = J_{Th} - A^p_{Th}\lambda_{Th} \quad (4)$$

where A^p_{Th} is the particulate ^{234}Th activity and P_{Th} is the net loss of ^{234}Th via particle sinking. Residence times of dissolved ^{234}Th (τ_d) and particulate ^{234}Th (τ_p) are given

Table 2
^{234}Th activities in the subtropical and tropical Atlantic Ocean

Depth (m)	Dissolved ^{234}Th (dpm l^{-1})	± error	Particulate ^{234}Th (dpm l^{-1})	± error	Nitex ^{234}Th (dpm l^{-1})	± error	Total ^{234}Th (dpm l^{-1})	± error	^{238}U (dpm l^{-1})	Th/U (%)
Station 10	*33°S40°W*									
10	2.08	0.14	0.381	0.038	0.0072	0.0004	2.46	0.14	2.48	99
20	2.14	0.14	0.411	0.050	0.0073	0.0009	2.56	0.15	2.48	103
50	1.70	0.11	0.446	0.026	0.0051	0.0010	2.15	0.11	2.48	87
110	2.10	0.14	0.358	0.028	0.0009	0.0002	2.46	0.14	2.47	100
250	2.26	0.14	0.185	0.023	0.0070	0.0004	2.45	0.14	2.45	100
500	2.26	0.15	0.131	0.017	0.0048	0.0003	2.40	0.15	2.40	100
Station 8	*16.3°S25°W*									
10	1.88	0.14	0.320	0.027	0.0105	0.0003	2.21	0.14	2.57	86
20	1.81	0.12	0.445	0.045	0.0112	0.0008	2.26	0.13	2.57	88
50	1.82	0.11	0.694	0.061	0.0084	0.0004	2.52	0.12	2.57	98
100	1.28	0.09	0.726	0.070	0.0122	0.0005	2.01	0.11	2.53	80
150	1.97	0.14	0.410	0.039	0.0061	0.0008	2.38	0.14	2.52	95
500	2.11	0.12	0.201	0.011	N/A	N/A	2.31	0.12	2.39	97

Station RFZ	*0.5°S20°W*									
10	1.61	0.09	0.266	0.030	0.0059	0.0003	1.88	0.10	2.48	76
20	1.18	0.10	0.476	0.036	0.0126	0.0001	1.66	0.11	2.48	67
50	2.13	0.15	0.448	0.044	0.0031	0.0003	2.58	0.15	2.51	103
100	2.38	0.15	0.438	0.042	0.0030	0.0002	2.83	0.16	2.47	114
150	1.99	0.15	0.314	0.031	0.0038	0.0001	2.30	0.16	2.45	94
500	2.20	0.10	0.255	0.021	0.0054	0.0009	2.46	0.10	2.38	103
Station 6	*8°N45°W*									
10	1.49	0.10	0.153	0.016	0.0139	0.0003	1.65	0.11	2.48	67
20	1.80	0.12	0.178	0.019	0.0114	0.0008	1.99	0.12	2.48	80
50	1.85	0.09	0.199	0.022	0.0051	0.0002	2.05	0.09	2.49	82
100	1.71	0.12	0.465	0.041	0.0034	0.0001	2.17	0.13	2.50	87
150	2.33	0.13	0.295	0.031	0.0018	0.0002	2.62	0.13	2.48	106
500	2.41	0.15	0.252	0.023	0.0018	0.0001	2.66	0.15	2.39	111
Station AMZ	*6°N48°W*									
1	0.56	0.04	0.294	0.032	0.0094	0.0002	0.86	0.05	2.19	39
20	1.81	0.07	0.156	0.017	0.0107	0.0001	1.97	0.07	2.48	80
50	1.61	0.08	0.489	0.039	0.0023	0.0003	2.10	0.09	2.51	84
100	1.50	0.09	0.589	0.053	0.0021	0.0001	2.10	0.10	2.52	83
150	1.84	0.09	0.464	0.041	0.0027	0.0001	2.31	0.09	2.51	92
500	2.04	0.12	0.285	0.030	0.0015	0.0002	2.33	0.12	2.39	97

Errors for ^{234}Th were propagated from counting statistics and Mn cartridge collection efficiency (for dissolved ^{234}Th).

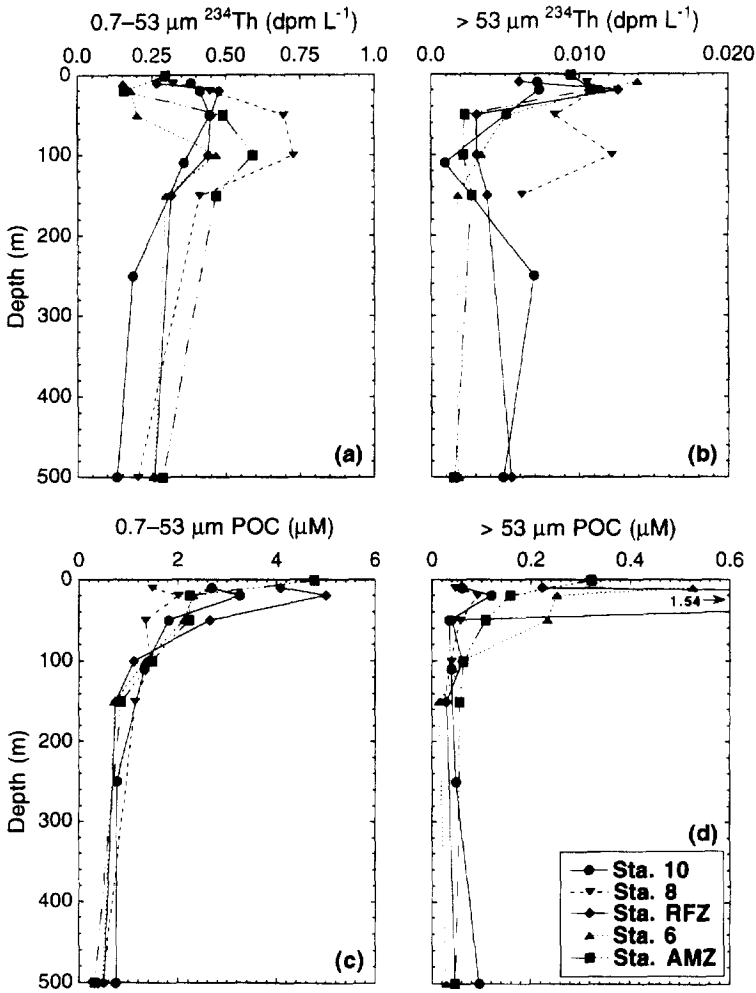

Fig. 4. Depth profiles of (a) 0.7–53-μm particulate ^{234}Th, (b) > 53-μm ^{234}Th, (c) 0.7–53-μm POC, and (d) > 53-μm POC.

by,

$$\tau_d = A^d_{Th}/J_{Th} = 1/k_1^* \tag{5}$$

and

$$\tau_p = A^p_{Th}/P_{Th} = 1/k_2^* \tag{6}$$

where k_1^* represents the scavenging rate constant for dissolved ^{234}Th, and k_2^* is the rate constant for the removal of ^{234}Th from surface waters on particles (Coale and Bruland, 1987).

Table 3
^{234}Th activities from the depth-integrated stations

Lat (deg N)	Long (deg W)	Diss. ^{234}Th (dpm l^{-1})	± error	Part. ^{234}Th (dpm l^{-1})	± error	Nitex ^{234}Th (dpm l^{-1})	± error	Total ^{234}Th (dpm l^{-1})	± error	^{238}U (dpm l^{-1})	Th/U (%)
5.8	31	1.67	0.11	0.301	0.040	0.0068	0.0008	1.98	0.12	2.46	80
4.5	22	1.46	0.10	0.318	0.027	0.0122	0.0002	1.79	0.10	2.46	73
2.5	21	2.24	0.14	0.230	0.025	0.0110	0.0006	2.49	0.14	2.44	102
−2.5	21	1.54	0.13	0.326	0.039	0.0045	0.0008	1.88	0.14	2.47	76
−4.5	22	1.59	0.11	0.271	0.028	0.0186	0.0005	1.89	0.12	2.48	76
−10	23	2.07	0.13	0.565	0.054	0.0044	0.0002	2.64	0.14	2.52	105

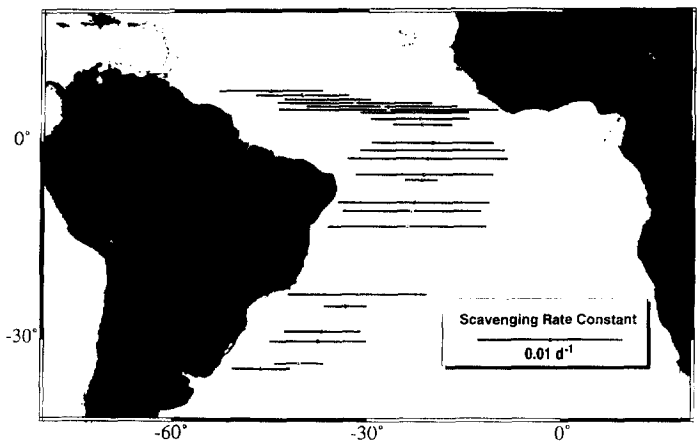

Fig. 5. Scavenging rate constants (k_f^*) for dissolved ^{234}Th (< 1μm) in the surface waters (~ 3 m) along the cruise track. Samples were collected using the ship's seawater intake.

The average residence time for particulate ^{234}Th in the surface waters was 14 days ($n = 23$; Table 1). The τ_p values fell into two categories: a mean of 29 days ($n = 9$) from 33°S to 10°S, which we attribute to the low particle export within this oligotrophic gyre. In the central South Atlantic (6°S to 10°N) the mean τ_p was 4.9 days ($n = 14$), coinciding with the higher productivity of equatorial waters. Residence times were shortest between 5°N and 6°N, where they averaged 1.7 days ($n = 3$).

Unlike particulate ^{234}Th, the residence times for dissolved ^{234}Th were similar in oligotrophic and equatorial regions (Fig. 5). Along the entire cruise track, τ_d averaged 164 ± 98 days but was low between 5°N and 6°N, with a mean τ_d of 86 days. The shorter residence times between 5°N and 6°N may be due to enhanced particle scavenging of ^{234}Th on Saharan dust. In support of this suggestion to, aeorsol filters from these stations were relatively dark in comparison to other stations (T.M. Church, per. comm.).

4.2. *Particulate organic carbon fluxes estimated from ^{234}Th*

Several studies have used ^{234}Th/^{238}U disequilibria to estimate POC export (Buesseler et al., 1992a; Cochran et al., 1995). To quantify the removal of POC, we need to know the export flux of ^{234}Th due to particle settling. The activity balance for total ^{234}Th is given by (Buesseler et al., 1992a),

$$\frac{d^{234}Th}{dt} = A_U\lambda_{Th} - A_{Th}\lambda_{Th} - P_{Th} \pm V \tag{7}$$

where V represents both horizontal advection and diffusion. Due to our limited sampling coverage in both space and time, we simplify this equation by making several assumptions: (1) ^{234}Th is removed on particles > 53 μm in diameter (= P_{Th});

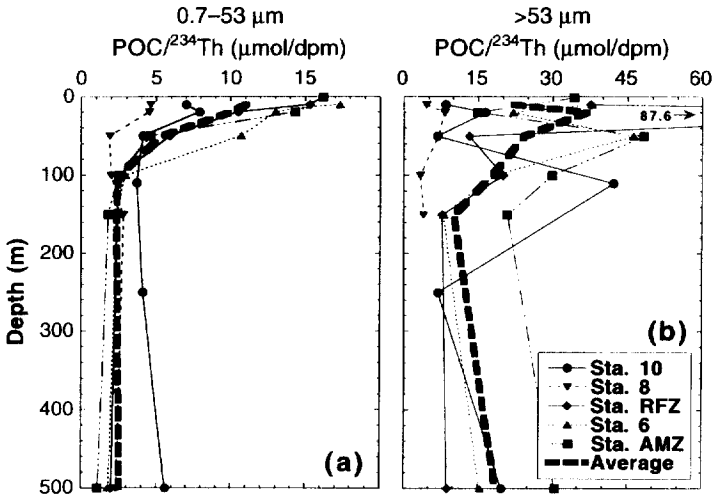

Fig. 6. Depth profiles of POC/^{234}Th ratios for the suspended (0.7–53-μm) and large particles (>53-μm). The thick dashed line represents the depth-averaged POC/^{234}Th ratio.

(2) ^{234}Th scavenging is at steady-state ($d^{234}Th/dt = 0$); (3) vertical processes dominate over horizontal advection and diffusion ($V \approx 0$), and; (4) ^{234}Th is removed primarily on biogenic particles. Eq. (7) can be simplified to the 1-D (vertical) model,

$$P_{Th} = \lambda_{Th} \int_0^z [A_U - A_{Th}]\, dz \tag{8}$$

where z is the depth at which P_{Th} is calculated. Trapezoidal integration was used to determine P_{Th}. Using the POC/^{234}Th ratio measured on the >53-μm fraction, we calculated the POC export flux (P_{POC}) using,

$$P_{POC} = \frac{POC}{^{234}Th_p} \times P_{Th}. \tag{9}$$

Because this is an empirical relationship, P_{POC} depends critically on the POC/^{234}Th ratio, but not that POC and ^{234}Th have similar residence times (Buesseler et al., 1992a; Bacon et al., 1996).

Several studies have observed a decrease in the POC/^{234}Th ratio with depth (Buesseler et al., 1992a; Bacon et al., 1996; Rutgers van der Loeff et al., 1997). Measurements of POC/^{234}Th in sediment traps during the North Atlantic Bloom Experiment indicate that the ratio doubled during the experiment (~1 month) (Buesseler et al., 1992a). A compilation of POC/^{234}Th ratios, from colloids (~1–10 nm) to particles >53-μm in size, exhibited a trend of decreasing POC/^{234}Th ratios with increasing particle size (Moran et al., 1993). Although we only collected two sizes of particles, the opposite trend was observed – i.e. an increase in POC/^{234}Th with increasing particle size (Fig. 6). Previous workers have used the POC/^{234}Th ratio on the larger particles, collected on 53-μm Nitex screen (Buesseler et al., 1995;

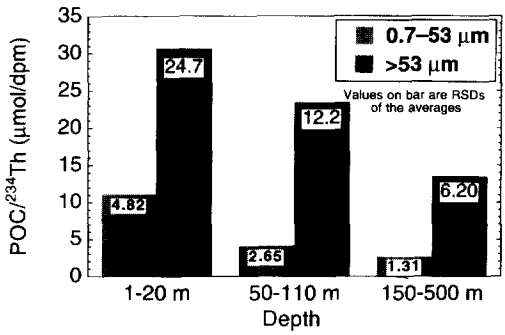

Fig. 7. POC/^{234}Th ratios grouped and averaged for discrete depth ranges. Values in each bar represent the standard deviation.

Bacon et al., 1996) and in sediment traps (Buesseler et al., 1992a; Murray et al., 1996), which are believed to be responsible for the bulk of the rapid export of particulate organic matter. We used the POC/^{234}Th ratio on the $>$ 53-μm particles at each depth to calculate POC export fluxes.

In a parcel of water within the euphotic zone, coagulation and heterotrophic grazing may explain a given trend between POC/^{234}Th and particle size. Decay of particulate ^{234}Th as particles age may also be important (Burd et al., 1999). In general, we would expect growth to dominate in the upper layers and grazing and radioactive decay of ^{234}Th to become more important at depth. This explanation would account for the observed decrease in the POC/^{234}Th ratio with depth and particle size. At Station RFZ, where POC/^{234}Th ratios were particularly high in the surface waters, we examined the $>$ 53-μm particulate fraction using a microscope. In addition to detritus, we found an abundance of *Ceratium spp.*, the largest species of dinoflagellate ($\sim$ 200 μm). Fig. 7 shows average POC/^{234}Th ratios from three depth ranges. The ratio decreased with depth and is greater in the $>$ 53-μm fraction at all depths. Because we expect ^{234}Th to be associated with the particle surface and POC with the volume of a particle, these observations are consistent with the greater volume-to-surface ratio of large particles.

It is interesting that the POC/^{234}Th ratios are large in comparison to other recent studies (Buesseler et al., 1995; Bacon et al., 1996; Murray et al., 1996). For example, Murray et al. (1996) found that the ratio on in situ pump samples (1–53 μm and $>$ 53 μm) tended to be low, between 1–5 μmol/dpm, and similar in magnitude on both size fractions. They also calculated a POC/^{234}Th ratio from Niskin bottle filtration (GF/F-POC/Nuclepore-^{234}Th) which ranged from 2–14 μmol/dpm and was consistently higher than ratios from large-volume in situ filtration. This observation suggests that different sampling techniques, i.e. bottle vs. in situ filtration, may yield different POC/^{234}Th ratios. These differences may be related to bottle vs. large-volume pumping POC concentrations rather than differences in particulate ^{234}Th activity. The large amount of seawater filtered by in situ pumps or, in our case, a rosette configured for collecting large volumes usually results in a filter with

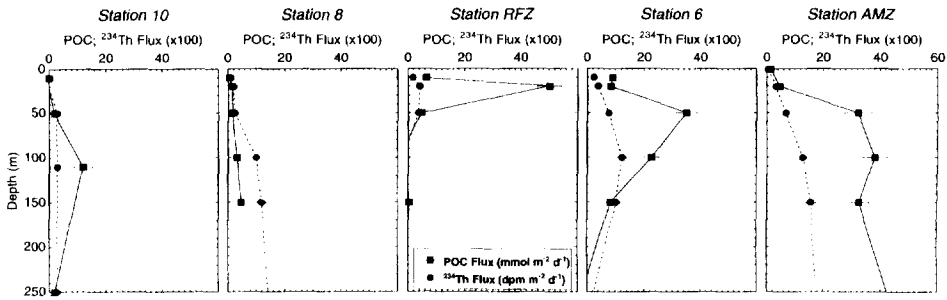

Fig. 8. Profiles of POC and ^{234}Th export for the five major stations.

a significantly higher POC concentration relative to the filter blank than would be found on a bottle filtration using a 25 mm GF/F. A carbon blank, for example from DOC adsorption during filtration, the combusted filter, or from the elemental analyzer, will add significantly to the error on a small volume filtration for estimating POC and thus the POC/^{234}Th ratio.

Eq. (9) was used to calculate the POC flux as a function of depth (Fig. 8) and the profiles calculated using the integrated ^{234}Th deficit and the corresponding POC/^{234}Th ratio. For Station 10, the net export of POC was low throughout the upper euphotic zone, with a maximum in the POC flux of 12 mmol C m^{-2} d^{-1} at 110 m (decreasing to 2.0 mmol C m^{-2} d^{-1} at 250 m). At Station 8, POC export was 4.6 mmol C m^{-2} d^{-1} (150 m). At stations 8 and 10, the maximum in the POC export flux was deeper in the water column. At these stations, the upper layers showed a high degree of particle recycling, while the lower layers were more eutrophic, most likely zones of higher export production.

Near the equator (Station RFZ), POC export was confined to the upper 150 m. The flux increased from 6.5 mmol C m^{-2}d^{-1} at 10 m to a maximum of 50 mmol C m^{-2} d^{-1} at 20 m, then declined to near zero at 150 m. Nearly 90% of the POC exported at 20 m was remineralized by 50 m. A similar distribution of POC export has been observed in the equatorial Pacific Ocean, with maxima between 60 and 80 m during Spring and Fall (Bacon et al., 1996). Our model calculations for ^{234}Th export neglect advection which may be important at stations near the equator due to upwelling of water enriched in ^{234}Th. In the equatorial Pacific, Buesseler et al. (1995) found that ^{234}Th fluxes were 25–35% higher when upwelling was considered. As a result, our estimates of POC export along the equator may represent the lower limit.

At Station 6, the POC flux was 8–9 mmol C m^{-2} d^{-1} in the upper 20 m and reached a maximum of 35 mmol C m^{-2} d^{-1} at 50 m. Over 75% of the POC exiting the upper 50 m was remineralized or consumed by 150 m. The highest POC fluxes were at Station AMZ, where values increased from 5.0 mmol C m^{-2} d^{-1} at 20 m to 38 mmol C m^{-2} d^{-1} at 100 m, then remained near 30 mmol C m^{-2} d^{-1} to 150 m. At Station AMZ, scavenging of ^{234}Th by inorganic particles may have lead to a higher apparent POC flux.

Table 4
Comparison of the depth-integrated and discrete profile sampling techniques for determining ^{234}Th-derived POC export fluxes

	0–100 m integrated	0–100 m profile
Diss. ^{234}Th (dpm l^{-1})	2.04 ± 0.12	1.68 ± 0.22
Part. ^{234}Th (dpm l^{-1})	0.240 ± 0.04	0.272 ± 0.06
Nitex ^{234}Th (dpm l^{-1})	0.0088 ± 0.0001	0.0074 ± 0.0007
0.7–53 μm POC (μM)	2.00	2.04
> 53 μm POC (μM)	0.272	0.274
Chl.-a (μg l^{-1})	0.25	0.24
Integrated ^{234}Th (dpm m^{-2} d^{-1})	605 ± 32	1230 ± 140
> 53 μm POC/Th (μmol/dpm)	31	18
POC export flux (mmol C m^{-2} d^{-1})	18.6 ± 1.0	22.6 ± 2.6

POC export from the depth-integrated sampling ranged from 16 to 43 mmol C m^{-2} d^{-1} at 5.75°N and 2.5°S, respectively. Fluxes at 4.5°S and 4.5°N were similar in magnitude, 23 and 28 mmol C m^{-2} d^{-1}, respectively. In contrast at 10°S and 2.5°N, ^{234}Th was in equilibrium with ^{238}U. As a result, we calculated an apparent POC export flux of zero.

To compare POC fluxes determined using discrete profiles with those from depth-integration, the integration technique was used at Station 6 where we had already collected a profile (Table 4 – the depth-integrated sample was collected within 36 h of the first sample from the profile). Good agreement existed between the two techniques for POC, > 53-μm POC, and Chl-a, and fair agreement in particulate ^{234}Th measurements. A significant disagreement was evident for dissolved ^{234}Th, with the depth-integrated activity being roughly 20% greater than the profile. Since the discrete profile only had samples collected from four depths in the upper 100 m versus six for the depth-integrated sample, we may have missed an important feature in the dissolved ^{234}Th profile.

4.3. *Export production in the equatorial Atlantic*

To assess the regional magnitude of export production in the equatorial Atlantic, the average POC export flux was calculated from our transect across the equator (17.8 mmol C m^{-2} d^{-1}; $n = 5$) and applied to the area from 5°S to 5°N and 25°W to 5°E (3.7×10^{12} m^2). Using these values, we estimate that approximately 0.29 Gt C yr^{-1} is exported from the Atlantic equator. From a recent estimate of average annual production in the eastern tropical Atlantic of 2.3 Gt C yr^{-1} (Monger et al., 1997), the average *e-ratio* for this region is 0.13. By comparison, export production in the equatorial Pacific has been estimated at 0.42 Gt C yr^{-1} (Murray et al., 1996). Combined, these regions account for over 8% of the annual global export production of 8.8 Gt C yr^{-1} (Six and Maier-Reimer, 1996).

4.4. Implications for the global carbon cycle

Estimates of POC export used in global carbon budgets are often derived from GCMs. For example, the Princeton modeling group has used globally distributed phosphate and dissolved organic nitrogen measurements, as well as the Redfield ratio to indirectly estimate POC export at ~ 100 m throughout the world's oceans (Najjar et al., 1992). It is desirable to provide direct measurements to check the distribution and magnitude of POC export estimated using GCMs. It should be noted that these model simulations provide annually averaged values of POC export for a given location, whereas the ^{234}Th-derived results provide an integrated measure of POC export on a time scale of days to weeks.

Several studies conducted in the Atlantic Ocean provide an opportunity to compare POC export estimated from GCMs with ^{234}Th-derived methods: (1) Bermuda Atlantic Time Series (BATS – Michaels et al., 1994), (2) North Atlantic Bloom Experiment (NABE – Buesseler et al., 1992a), and (3) German – JGOFS at the Antarctic Polar Front (APF – Rutgers van der Loeff et al., 1997). The BATS study, located at 32°N, 64°W, has included measurements of POC export over the upper 150 m since 1993; integrated ^{234}Th deficits were combined with the POC/^{234}Th ratio in sediment trap material from 150 m to calculate a POC flux. The NABE (47°N, 20°W) took place from April to May 1989. These investigators measured the POC/^{234}Th ratio in sediment trap material as well as on 0.7 μm filters. The German JGOFS expedition to the APF in the Atlantic, in October and November 1992, used measurements of POC (0.7 μm glass-fiber) and ^{234}Th (1 μm polycarbonate) on filters to obtain an average POC/^{234}Th ratio that was used to calculate a POC flux.

The Princeton GCM includes values for both new production (NP) and export production (EP) (Najjar, 1990). Export production is defined as the amount of organic carbon leaving the euphotic zone in particulate form. In the model, EP is NP minus DOC remineralization in the photic zone. The resolution of the model's output was 4.5° latitude by 3.75° longitude. Although the measurements are from different longitudes in the Atlantic,we have attempted to compare the model data with that predicted from ^{234}Th.

In most cases, the GCM is comparable with the ^{234}Th results (Fig. 9). In the Southern Ocean during the JGOFS expedition, bloom conditions were encountered in the austral spring and POC export was not at steady state (Rutgers van der Loeff et al., 1997). The maximum in export from the GCM near 40°S is not an open ocean feature, but rather an artifact of the grid approaching the productive waters near the South American coastline. Our maximum in the POC flux at 2.5°S coincides with the GCM maximum. Even the POC flux at NABE, measured before the onset of the bloom, agrees with the GCM. At 18°S and 33°N, within the oligotrophic gyres of their respective hemispheres, ^{234}Th-predicted fluxes are comparable. Fluxes that do not agree in magnitude with the GCM, such as at the Polar Front, may be an issue of temporal integration. Whereas the ^{234}Th-derived results were collected during different seasons, at present, the GCM predicts the average export on an annual basis.

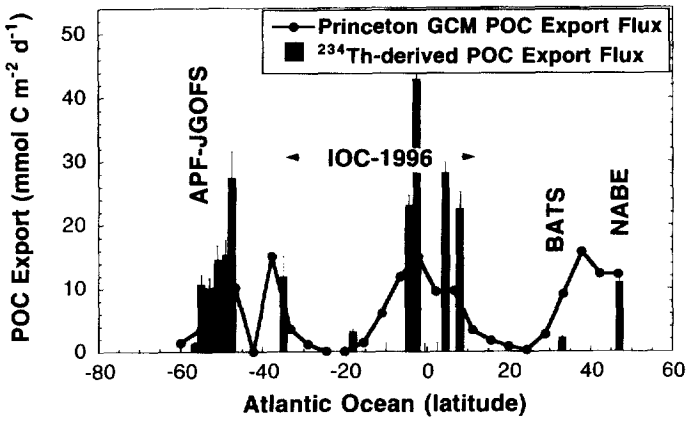

Fig. 9. POC export fluxes calculated using the Princeton GCM and the ^{234}Th tracer approach. All ^{234}Th-derived POC fluxes were integrated to a depth of ~ 100 m. (APF-JGOFS: Rutgers van der Loeff et al., 1997; BATS [Bermuda-Atlantic Time Series]: Michaels et al., 1994; NABE [North Atlantic Bloom Experiment]: Buesseler et al., 1992).

5. Conclusions

Rates of particle scavenging and POC export have been calculated using the natural tracer ^{234}Th. Relatively high ^{234}Th scavenging rates between 5°N and 6°N may indicate that this region was impacted by the transport of aeolian material from the Sahara. Annual export production in the equatorial Atlantic was estimated to be 0.29 Gt C yr^{-1}. Differences in particle export between the equatorial Atlantic, and Pacific are attributed to the larger POC/^{234}Th ratios measured in the Atlantic, we attribute this difference to the higher abundance of large phytoplankton cells in the Atlantic relative to the non-limited equatorial Pacific region. The ^{234}Th-derived POC export fluxes reported in this and other studies were comparable with results obtained from a GCM.

Acknowledgements

We wish to thank Greg Cutter for the invitation to participate on the IOC-96 cruise and for travel funds. M. Lavelle, M.M. Sarin, and G. Kim provided much assistance during long hours of sampling. Thanks to S. Zimmermann and R.C. Kidd for help with the CTD rosette. K. Grembowicz supplied the pigment data. Nutrient analyses were the courtesy of P. Clement. Thanks to R. Murnane for providing output from the Princeton GCM. B. Fitzgerald, K. Rolfhus, and T. Church provided additional logistical support. R. Pockalny provided graphical assistance with GMT. Finally, we wish to acknowledge the constructive reviews of K. Rahn, J. Murray, K. Buesseler, and one anonymous reviewer. We wish to thank the Intergovernmental Oceanographic Commission, the United States National Science Foundation (OCE-9523159

to G. Cutter), the Habitat Chemistry Section of the Marine Environmental Science Division of the Department of Fisheries and Oceans, Bedford Institute of Oceanography, and the Captain and crew of the R/V *Knorr* for their support of the IOC-1996 Expedition. This work was funded in part by an ONR Young Investigator Award to SBM (N00014-96-1-0685).

References

Bacon, M.P., Cochran, J.K., Hirschberg, D., Hammar, T.R., Fleer, A.P., 1996. Export flux of carbon at the equator during the EqPac time-series cruises estimated from ^{234}Th measurements. Deep-Sea Research II 43, 1133–1153.

Bhat, S.G., Krishnaswamy, S., Lal, D., Rama, Moore, W.S., 1969. ^{234}Th/^{238}U ratios in the ocean. Earth and Planetary Science Letters 5, 483–499.

Bishop, J.K.B., Edmond, J.M., Ketten, D.R., Bacon, M.P., Silker, W.B., 1977. The chemistry, biology, and vertical flux of particulate matter from the upper 400 m of the equatorial Atlantic Ocean. Deep-Sea Research 24, 511–548.

Bruland, K.W., Coale, K.H., 1986. Surface water ^{234}Th/^{238}U disequilibria: spatial and temporal variations of scavenging rates within the Pacific Ocean. In: Burton, J.D., Brewer, P.G., Chesselet, R. (Eds.), Dynamic Processes in the Chemistry of the Upper Ocean. Plenum Publishing Co., New York, pp. 159–172.

Buesseler, K.O., Bacon, M.P., Cochran, J.K., Livingston, H.D., 1992a. Carbon and nitrogen export during the JGOFS North Atlantic Bloom Experiment estimated from ^{234}Th:^{238}U disequilibria. Deep-Sea Research 39, 1115–1137.

Buesseler, K.O., Cochran, J.K., Bacon, M.P., Livingston, H.D., Casso, S.A., Hirschberg, D., Hartman, M.C., Fleer, A.P., 1992. Determination of thorium isotopes in seawater by non-destructive and radiochemical methods. Deep-Sea Research 39, 1103–1114.

Buesseler, K.O., Andrews, J.A., Hartman, M.C., Belastock, R., Chai, F., 1995. Regional estimates of the export flux of particulate organic carbon derived from thorium-234 during the JGOFS EqPac program. Deep-Sea Research 42, 777–804.

Burd, A., Moran, S.B., Jackson, G.A., 1999. A coupled adsorption-aggregation model of the POC/^{234}Th ratio of marine particles. Deep-Sea Research, in press.

Chen, J.H., Edwards, R.L., Wasserburg, G.J., 1986. ^{238}U, ^{234}U, and ^{232}Th in seawater. Earth and Planetary Science Letters 80, 241–251.

Coale, K.H., Bruland, K.W., 1985. ^{234}Th:^{238}U disequilibria within the California Current. Limnology and Oceanography 30, 22–33.

Coale, K.H., Bruland, K.W., 1987. Oceanic stratified euphotic zone as elucidated by ^{234}Th:^{238}U disequilibria. Limnology and Oceanography 32, 189–200.

Cochran, J.K., Barnes, C., Achman, D., Hirschberg, D.J., 1995. Thorium-234/Uranium-238 disequilibrium as an indicator of scavenging rates and particulate organic carbon fluxes in the Northeast Water Polynya, Greenland. Journal of Geophysical Research 100, 4399–4410.

Hartman, M.C., Buesseler, K.O., 1994. Adsorbers for In-situ collection and At-Sea Gamma Analysis of Dissolved Thorium-234 in Seawater (WHOI-94-15). Woods Hole Oceanographic Institution.

Livingston, H.D., Cochran, J.K., 1987. Determination of transuranic and thorium isotopes in ocean water: in solution and filterable particles. Journal of Radioanalytical and Nuclear Chemistry:Articles 115, 299–308.

Matsumoto, E., 1975. ^{234}Th-^{238}U radioactive disequilibrium in the surface layer of the ocean. Geochimica et Cosmochimica Acta 39, 205–212.

Michaels, A.F., Bates, N.R., Buesseler, K.O., Carlson, C.A., Knap, A.H., 1994. Carbon-cycle imbalances in the Sargasso Sea. Nature 372, 537–540.

Monger, B., McClain, C., Martugudde, R., 1997. Seasonal phytoplankton dynamics in the eastern tropical Atlantic. Journal of Geophysical Research 102, 12 389–12411.

Moran, S.B., Buesseler, K.O., Niven, S.E.H., Bacon, M.P., Cochran, J.K., Livingston, H.D., Michaels, A.F., 1993. Regional variability in size-fractionated C/^{234}Th ratios in the upper ocean: importance of biological recycling. The Oceanography Society, Seattle, WA.

Moran, S.B., Ellis, K.M., Smith, J.N., 1997. ^{234}Th/^{238}U disequilibrium in the central Arctic Ocean: implications for particulate organic carbon export. Deep-Sea Research II 44, 1593–1606.

Murray, J.W., Barber, R.T., Roman, M.R., Bacon, M.P., Feely, R.A., 1994. Physical and biological controls on carbon cycling in the Equatorial Pacific. Science 266, 58–65.

Murray, J.W., Young, J., Newton, J., Dunne, J., Chapin, T., Paul, B., McCarthy, J.J., 1996. Export flux of particulate organic carbon from the central equatorial Pacific determined using a combined drifting trap-^{234}Th approach. Deep-Sea Research II 43, 1095–1132.

Najjar, R.G., 1990. Simulations of the phosphorous and oxygen cycles in the world ocean using a General Circulation Model. Ph.D. Thesis, Princeton University,

Najjar, R.W., Sarmiento, J.L., Toggweiler, J.R., 1992. Downward transport and fate of organic matter in the ocean: simulations with a general circulation model. Global Biogeochemical Cycles 6, 45–76.

Pike, S.M., Moran, S.B., 1997. Use of Poretics 0.7 μm pore size glass fiber filters for determination of particulate organic carbon and nitrogen in seawater and freshwater. Marine Chemistry 57, 355–360.

Rutgers van der Loeff, M.M., Friedrich, J., Bathmann, U.V., 1997. Carbon export during the spring bloom at the Antarctic Polar Front, determined with the natural tracer ^{234}Th. Deep-Sea Research 44, 457–478.

Six, K.D., Maier-Reimer, E., 1996. Effects of plankton dynamics on seasonal carbon fluxes in an ocean general circulation model. Global Biogeochemical Cycles 10, 559–583.